Carcinogenesis, 2020, Vol. 41, No. 8, 1134–1144

doi:10.1093/carcin/bgz190
Advance Access Publication November 19, 2019
Original Article

ORIGINAL ARTICLE

Osteopontin drives *KRAS*-mutant lung adenocarcinoma

Ioanna Giopanou[1,*], Nikolaos I.Kanellakis[1], Anastasios D.Giannou[1], Ioannis Lilis[1], Antonia Marazioti[1], Magda Spella[1], Vassilios Papaleonidopoulos[1], Davina C.M.Simoes[2], Dimitra E.Zazara[1], Theodora Agalioti[1], Charalampos Moschos[3], Sophia Magkouta[3], Ioannis Kalomenidis[3], Vily Panoutsakopoulou[4,†], Anne-Sophie Lamort[5], Georgios T.Stathopoulos[1,5,‡] and Ioannis Psallidas[1,6,7,‡]

[1]Laboratory for Molecular Respiratory Carcinogenesis, Department of Physiology, Faculty of Medicine, University of Patras, Rio, Achaia, 26504, Greece, [2]Department of Applied Sciences, Faculty of Health and Life Sciences, Northumbria University Newcastle, Newcastle Upon Tyne, UK, [3]"Marianthi Simou Laboratory," 1st Department of Critical Care and Pulmonary Medicine, National and Kapodistrian University of Athens, School of Medicine, Evangelismos Hospital, 10675 Athens, Greece, [4]Cellular Immunology Laboratory, Center for Basic Research, Biomedical Research Foundation of the Academy of Athens, Athens 11527, Greece, [5]Comprehensive Pneumology Center (CPC) and Institute for Lung Biology and Disease (iLBD), University Hospital, Ludwig-Maximilians University and Helmholtz ZentrumMünchen, Member of the German Center for Lung Research (DZL), Munich, Bavaria, 81377, Germany, [6]Oxford Centre for Respiratory Medicine, Oxford University Hospitals NHS Trust, Oxford, UK and [7]Lungs for Living Research Centre, UCL Respiratory, University College London, London, UK

*To whom correspondence should be addressed. Ioanna Giopanou, Faculty of Medicine, University of Patras, 1 Asklepiou Str., University Campus, 26504 Rio, Greece. Tel: +302610969154; Fax: +302610969176; Email: giopanou@upatras.gr
†Deceased.
‡Co-senior authors.
Correspondence may also be addressed to Georgios T. Stathopoulos, Faculty of Medicine, University of Patras, 1 Asklepiou Str., University Campus, 26504 Rio, Greece. Email: gstathop@upatras.gr

Abstract

Increased expression of osteopontin (secreted phosphoprotein 1, SPP1) is associated with aggressive human lung adenocarcinoma (LADC), but its function remains unknown. Our aim was to determine the role of SPP1 in smoking-induced LADC. We combined mouse models of tobacco carcinogen-induced LADC, of deficiency of endogenous *Spp1* alleles, and of adoptive pulmonary macrophage reconstitution to map the expression of SPP1 and its receptors and determine its impact during carcinogenesis. Co-expression of *Spp1* and mutant $Kras^{G12C}$ in benign cells was employed to investigate SPP1/KRAS interactions in oncogenesis. Finally, intratracheal adenovirus encoding *Cre* recombinase was delivered to $LSL.KRAS^{G12D}$ mice lacking endogenous or overexpressing transgenic *Spp1* alleles. SPP1 was overexpressed in experimental and human LADC and portended poor survival. In response to two different smoke carcinogens, *Spp1*-deficient mice developed fewer and smaller LADC with decreased cellular survival and angiogenesis. Both lung epithelial- and macrophage-secreted SPP1 drove tumor-associated inflammation, while epithelial SPP1 promoted early tumorigenesis by fostering the survival of *KRAS*-mutated cells. Finally, loss and overexpression of *Spp1* was, respectively, protective and deleterious for mice harboring $KRAS^{G12D}$-driven LADC. Our data support that SPP1 is functionally involved in early stages of airway epithelial carcinogenesis driven by smoking and mutant *KRAS* and may present an important therapeutic target.

Introduction

Lung cancer is the leading cancer killer, claiming 1.73 million lives and 36 million years of life lost worldwide in 2015 alone and lung adenocarcinoma (LADC) constitutes the deadliest human neoplasm *per se* (1,2). Although 15% of LADC cases occur

Received: April 13 2019; **Revised:** October 15 2019; **Accepted:** November 18 2019

Abbreviations

BAL	bronchoalveolar lavage
BHT	butylatedhydroxytoluene
CANTOS	Canakinumab Anti-inflammatory Thrombosis Outcomes Study
LADC	lung adenocarcinoma
MCA	3-methylcholanthrene
PCNA	proliferating cell nuclear antigen
PFU	plaque-forming units
SPP1	secreted phosphoprotein 1
STR	short tandem repeats

in never smokers, tobacco smoking is the leading risk factor for LADC (3,4). LADC of smokers most frequently harbor mutations in the KRAS protooncogene GTPase (*KRAS*), which are notoriously undruggable. Patients with *KRAS*-mutant LADC are in need for new targeted therapies that prerequisite a deeper understanding of the pathobiology of the disease (5,6). Osteopontin (secreted phosphoprotein 1, SPP1; encoded by the human/murine *SPP1*/*Spp1* genes), is a secreted, chemokine-like, matricellular phosphoglycoprotein that is widely expressed in the human body (7). Although SPP1 facilitates physiologic processes, it has also been shown to drive tumor progression in mouse models of different metastatic cancers (8–12). Elevated SPP1 expression has been associated with worse lung cancer patients prognosis (13) and its knock-down inhibited the growth of lung cancer cell lines (11,14). Importantly, deficiency in the SPP1 receptor CD44 and exogenous delivery of non-functional decoy SPP1 were protective in genetic mouse models of LADC (15,16). However, the functional role of SPP1 in physiologically relevant mouse models of *de novo* development of LADC in response to tobacco chemicals (17,18) has not been studied.

The aim of this study was to map and investigate the functional role of SPP1, and to identify its action during *de novo* LADC development in response to tobacco carcinogens. For this, multiple mouse models of SPP1 deficiency and overexpression were deployed in combination with cellular models of survival competition. The results demonstrate the importance of SPP1 in early stages of cell-autonomous lung tumor formation and progression and provide a direct link between *KRAS* mutations and the tumorigenic activity of SPP1, positioning SPP1 as a therapeutic target against *KRAS*-mutant LADC.

Materials and methods

Additional details can be found in the supplementary information material at http://carcin.oxfordjournals.org/.

Ethics approval

Experiments were carefully designed and preapproved by the Veterinary Administration of the Prefecture of Western Greece (approvals #3741/16.11.2010, 60291/3035/19.03.2012, and 118018/578/30.04.2014) and conducted according to Directive 2010/63/EU (http://eur-lex.europa.eu/LexUriServ/LexUriServ.do?uri= OJ:L:2010:276:0033:0079:EN:PDF).

Human data

BATTLE study microarrays were from GEO series GSE43458 (19). *SPP1*/*ACTB* transcript abundance was determined for each patient using Affymetrix (Santa Clara, CA) software. Survival was analyzed on Kaplan–Meier Plotter (http://kmplot.com/analysis/ (20)) using: probe ID = 209875_s_at; auto-select best cut-off; compute median survival; histologic subtype = All or LADC; Cox regression = multivariate including AJCC stages T and N.

Cell line authedication

Human HEK293T embryonic kidney cells were a generous gift from Professor's Ioannis Kalomenidis laboratory in January 2016. Primary LADC cells were isolated from urethane-induced LADC of *FVB* mice in our laboratory as described previously (21). All cell lines were tested biannually using short tandem repeats (STR) and *Mycoplasma* Spp. PCR and were cultured at 37°C in 5% CO_2-95% air using DMEM/10% FBS/2 mM L-glutamine/1 mM pyruvate/100 U/ml penicillin/100 mg/ml streptomycin. Cells were used for experiments after five passages.

Vectors and cell treatments

Plasmids used ((21–24); http://www.addgene.org/Georgios_Stathopoulos/; ID's in parentheses) include p*C* (6691 Bicistronic_ires_puro; 64335), p*Spp1* (pSpp1-is2; 58248), p*RFP* (Plenti-CMV-MCS-RFP-SV-puro; 109377; gift from Jonathan Garlick and Behzad Gerami-Naini), p*GFP* (7432 Bicistronic_GFP_ires_puro; 64336), p*GFP.Kras*^{G12C} (8027_GFP-KrasG12C_2B_puro; 64372), and p*Cag.Luc* (Cag.Luc.puro; 74409). Cells were transfected with 5 μg DNA using calcium phosphate. Stable clones were selected using puromycin (1–7 μg/ml). Cells were treated with daily recombinant murine SPP1 (rmSPP1; 40 ng/ml; #441-OP-050; R&D Systems, Minneapolis, MN) or neutralizing SPP1 antibodies (α-SPP1; 10 μg/ml; anti-mouse #ab11503, Abcam, Cambridge, MA; anti-human AF1433, R&D Systems, Minneapolis, MN).

Mouse models of LADC

C57BL/6J (*C57BL/6*; #000664), B6.129S6-*Spp1*^{tm1Blh}*/J* (*Spp1*$^{-/-}$; #004936; (25)), *FVB/NJ* (*FVB*; #001800), B6.129S4-*Kras*^{tm4Tyj}*/J* (*LSL.KRAS*^{G12D}; #008179; (26)),FVB-Tg$^{(CAG\text{-}luc,\text{-}GFP)L2G85Chco}$*/J*(*CAG-luc-eGFP*; #008450; (27)), and NOD.CB17-*Prkdc*$^{<scid>}$*/J* (*NOD/SCID*; #001303; (28)) mice from Jackson Laboratories and *Spp1-stop*$^{f/f}$*/CreER*^{T1}(*LSL.Spp1*^{Tg}; (29)) mice were bred in the University of Patras Center for Animal Models of Disease (for mouse numbers, see Supplementary Table 1, available at *Carcinogenesis* Online). LADC was induced in *FVB* mice using a single (*CAG-luc-eGFP* mice) or four (wild-type *FVB* mice) consecutive weekly intraperitoneal injections of 1 g/kg urethane (CAS#51-79-6; Sigma–Aldrich; St. Louis, MO) and in *C57BL/6* mice using 10 weekly injections (17,22). Alternatively, LADC was triggered in *C57BL/6* mice by four consecutive weekly intraperitoneal injections of 15 mg/kg 3-methylcholanthrene (MCA; CAS#56-49-5; Sigma) followed by six consecutive weekly intraperitoneal injections of 200 mg/kg butylatedhydroxytoluene (BHT; CAS#128-37-0; Sigma (30)). Experimental mice were sex-, weight (20–25 g)-, and age (6–12 week)-matched, were initiated on treatments at 6 weeks of age, and were sacrificed 4 months (*FVB* mice), 1 or 6 months (*C57BL/6* mice), or 2 weeks (*CAG-luc-eGFP* mice) following treatment. *KRAS*^{G12D}-driven LADC was induced via intratracheal delivery of 5×10^8 plaque-forming units (PFU) of adenovirus type 5 encoding CRE recombinase (Ad-*Cre*; Vector Development Lab, Baylor College of Medicine; Houston, TX) to *LSL.KRAS*^{G12D} mice (26). For flank oncogenesis, *NOD/SCID* mice received 2×10^6 subcutaneous HEK293T cells and vertical tumor diameters (δ) were measured. Mice were imaged for bioluminescent detection of cell mass weekly thereafter. Cell spot volume (*V*) was calculated as $V = \pi \times (\delta 1 \times \delta 2 \times \delta 3)/6$. For LADC development following adoptive alveolar macrophage reconstitution, *FVB* mice received total-body irradiation (900 rad) followed 12 h later by 10^7 intravenous bone marrow cells obtained from the four long bones of *Spp1*$^{+/+}$ or *Spp1*$^{-/-}$ mice, 1 month thereafter by intratracheal clodronate (0.5 mg in 100 μl), and yet another month thereafter by four consecutive weekly intraperitoneal urethane (1 g/kg) injections (23,31).

Imaging

For bioluminescence imaging, cells and mice were serially imaged on an Xenogen Lumina II after delivery of 300 μg/ml D-luciferin (Gold Biotechnology; St. Louis, MO) to culture media or 1 mg intravenous D-luciferin into the retroorbital veins. Data were analyzed using Living Image v.4.2 (Perkin-Elmer, Waltham, MA; (17,22,23)).

Statistics

Sample size (*n*; always biological) was determined using G*power (32), assuming $\alpha = 0.05$, $\beta = 0.05$, and $d = 1.5$. Data were acquired by two blinded readers, reevaluated if >20% deviant (no data were excluded), examined for normality by Kolmogorov–Smirnov test, and presented and analyzed as appropriate. Differences in frequencies were examined by χ^2 test, in means by *t*-test or one-way ANOVA/Tukey's post-tests, in medians by Mann–Whitney test or Kruskal–Wallis/Dunn's post-tests, in measurements over time by 2-way ANOVA/Bonferroni post-tests, and in survival by Kaplan–Meier estimates/log-rank tests and Cox regression. Probability (*P*)

is two-tailed and $P < 0.05$ was considered significant. Statistics and plots were done on Prism v5.0 (GraphPad, La Jolla, CA).

Results

SPP1 is overexpressed in LADC and portends poor survival

To assess SPP1 as a candidate driver of human LADC, we determined its expression in a well-defined microarray study of 30 normal lung samples and 80 LADC tissues from the BATTLE study (https://www.ncbi.nlm.nih.gov/geo/query/acc.cgi?acc=GSE43458; (19)). Raw data of each patient were analyzed separately and normalized to *ACTB* housekeeping transcripts, revealing marked overexpression of *SPP1* in LADC compared with normal lung tissue (Figure 1A). This fact was corroborated using The Human Protein Atlas (https://www.proteinatlas.org/ENSG00000118785-SPP1/pathology; (33)). In line with published studies (13,34,35), high SPP1 expression was also an unfavorable prognostic marker for 1150 patients with lung cancer and 231 patients with LADC from the Kaplan–Meier Plotter database (Figure 1B and C). We next sought to map SPP1 expression in chemical-induced LADC of mice, which features a mutation profile that is highly similar to human LADC (18). For this, *C57BL/6* mice competent (*Spp1*$^{+/+}$), haploinsufficient (*Spp1*$^{+/-}$), or deficient (*Spp1*$^{-/-}$) in *Spp1* alleles received 10 consecutive intraperitoneal injections of urethane (1 g/kg) and were examined for immunohistochemical detection of SPP1 immunoreactivity of lung tissues together with untreated *Spp1*-competent mice. In naïve mice, SPP1 expression was restricted to non-ciliated airway epithelial (club or Clara) cells (Figure 1D). In tumor-bearing lungs of *Spp1*-competent mice, SPP1 was highly and ubiquitously overexpressed in lung tumors, airway and alveolar epithelial cells, and alveolar macrophages; no SPP1 immunoreactivity was evident in the lungs from *Spp1*-deficient mice or when primary antibody was omitted (Figure 1E). A time-course experiment examining SPP1 protein levels in bronchoalveolar lavage (BAL) from urethane-treated *Spp1*$^{+/+}$, *Spp1*$^{+/-}$, and *Spp1*$^{-/-}$ mice by ELISA corroborated the progressively increasing release of SPP1 into the airspaces of urethane-treated *Spp1*$^{+/+}$ mice and validated SPP1 deficiency of both *Spp1*$^{+/-}$ and *Spp1*$^{-/-}$ mice (Figure 1F). Similar results were obtained when RNA extracted from LADC cells isolated from urethane-induced lung tumors (21,24), from lungs of naïve mice, and from lungs of urethane-treated mice (1 week latency) was analyzed by microarray and qPCR. These analyses corroborated the overexpression of *Spp1*, and also identified *Itgav*, *Itgb1*, *Itgb3*, *Itgb5*, and *Cd44* as the main SPP1 receptors overexpressed by LADC cells relative to *Gusb* housekeeping transcript (Figure 1G and H). The ITGB3 protein overexpression by LADC cells was also evident by immunofluorescence (Figure 1I). Collectively, these findings supported that SPP1 signaling may be important in LADC biology and warranted further investigation.

SPP1 promotes chemical-induced LADC in mice

To define the impact of SPP1 in LADC, we exposed *Spp1*$^{+/+}$, *Spp1*$^{+/-}$, and *Spp1*$^{-/-}$ mice (*C57BL/6*) to 10 repetitive urethane treatments and waited 6 months in order to generate chemical-induced LADC with *Kras* mutations (22). As shown in Figure 2A–F, *Spp1*$^{-/-}$ mice were markedly resistant to lung tumor induction compared with *Spp1*$^{+/+}$ mice, and *Spp1*$^{+/-}$ mice showed a phenotype closely resembling *Spp1*$^{-/-}$ mice, in line with their almost complete SPP1 protein deficiency in BAL (Figure 1F). *Spp1*$^{+/+}$ and *Spp1*$^{-/-}$ mice were also exposed to a second two-hit chemical carcinogen model of repetitive MCA-BHT injections, with similar results indicating marked resistance of *Spp1*-gene-deficient mice to chemical lung tumor induction (Figure 2G–L). To identify how SPP1 functions as tumor promoter, we further studied parameters of inflammation, cellular proliferation, apoptosis, and angiogenesis in the lungs of mice. To this end, *Spp1*$^{-/-}$ mice had fewer inflammatory cells in BAL, more PCNA+ and TUNEL+ cells in lung tumors, and fewer F8A+ angiogenic hotspots in lung tumors compared with *Spp1*$^{+/+}$ mice (Figure 3). The decreased proliferation/apoptosis ratio of lung tumors from *Spp1*$^{-/-}$ mice (determined as the ratio of PCNA+ dividing to TUNEL+ apoptotic cells) indicated that the enhanced cell proliferation observed was a rebound effect caused by the massive apoptotic rates they displayed (Figure 3G). Taken together, these results show that SPP1 promotes carcinogen-induced inflammation, cell proliferation, and angiogenesis, culminating in net tumor promotion at late stages post-carcinogen exposure.

Epithelial-derived SPP1 fosters cellular proliferation in the preneoplastic lung

The multifaceted phenotype of tumor-bearing *Spp1*$^{-/-}$ mice could be attributed to decreased epithelial proliferation at early stages of carcinogenesis leading to less progressed tumors causing less inflammation and angiogenesis (cell-autonomous effects of epithelial SPP1), or to tumor-promoting effects of tumor-infiltrating immune cells during late stages of carcinogenesis (paracrine effects of myeloid SPP1). To determine the mechanism, we performed two experiments. First, *Spp1*$^{+/+}$, *Spp1*$^{+/-}$, and *Spp1*$^{-/-}$ mice (*C57BL/6*) received four repetitive urethane treatments and were sacrificed prematurely thereafter (Figure 4A). In this model of early lung carcinogenesis (37), *Spp1*$^{-/-}$ mice displayed decreased inflammatory cells in BAL, fewer alveolar hyperplastic lesions, and statistically significantly fewer proliferating cells in hyperplastic lesions and airway epithelium (Figure 4B–F). In a second experiment aimed at dissecting epithelial- versus myeloid-SPP1 effects, wild-type FVB mice were subjected to total-body irradiation (900 rad) followed by adoptive bone marrow transfer of 10 million whole bone marrow cells obtained from *Spp1*$^{+/+}$ and *Spp1*$^{-/-}$ donors (23,24). One month later, when the native bone marrow was fully reconstituted by the transplants, all chimeric mice received intratracheal clodronate dosed to kill their alveolar macrophages, a technique previously shown to efficiently repopulate the lungs with bone marrow-derived macrophages (31). Yet another month thereafter, all animals with *Spp1*-competent lung epithelium and either *Spp1*-competent or -deficient lung myeloid cells were exposed to four consecutive urethane injections according to an accelerated tumorigenesis protocol (Figure 4G; (17)). Lung examination revealed no differences in tumor incidence, multiplicity or size between chimeric mice with *Spp1*$^{+/+}$ and *Spp1*$^{-/-}$ alveolar macrophages (achieved power 91%) but showed that the latter mice exhibited statistically significantly decreased numbers of BAL inflammatory cells (Figure 4H–L). This experiment showed that epithelial-derived SPP1 drives chemical-induced LADC, while both epithelial- and myeloid-derived SPP1 drive tumor-associated inflammation, consistent with results from transplantable cancer models (10,11). Collectively, the results indicate that epithelial-expressed SPP1 has a significant role in the establishment of clusters of proliferating cells with tumorigenic characteristics at early stages of lung carcinogenesis.

SPP1 drives the survival of *KRAS*-mutant cells

Since chemical-induced lung tumors of mice are *Kras*-mutant (18,22), and based on the above results that supported cell-autonomous effects of epithelial SPP1, we sought to test the impact of SPP1 on cell proliferation in the cellular contexts of wild-type versus mutant *Kras*. For this reason we decided to

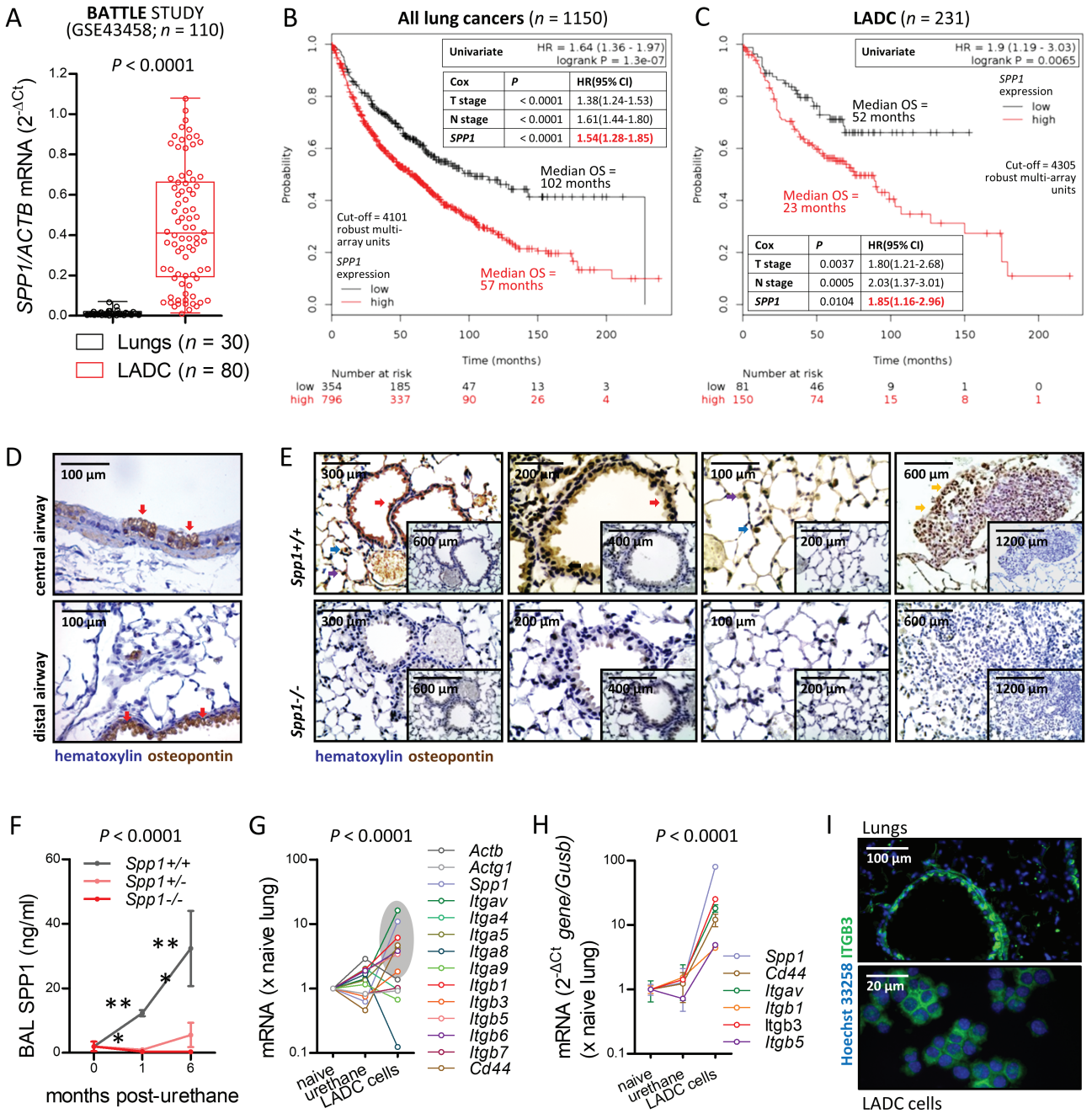

Figure 1. Secreted phosphoprotein 1 (SPP1) is overexpressed in human and murine lung tumors and is associated with poor survival. (**A**) SPP1 corrected for housekeeping ACTB transcript abundance using the $^{-}\Delta$CT method on microarray data from 30 normal lung and 80 lung adenocarcinoma (LADC) samples from the BATTLE study (GSE43458; (19)). Circles, data points; lines, median; boxes, interquartile range; bars, 50% outer quartiles; *n*, sample size; *P*, Mann–Whitney *U*-test probability. (**B** and **C**) Kaplan–Meier and Cox proportional hazards overall survival (OS) analyses of 1150 patients with lung cancer (**B**) and 231 patients with LADC (**C**) stratified into low (black) and high (red) SPP1 transcript expression by optimal cut-offs shows that SPP1 overexpression is a stage-independent negative predictor of OS. Lines and numbers, Kaplan–Meier survival plots and risk estimates; *P* and HR, univariate Kaplan–Meier and multivariate Cox-regression probabilities (*P*) and hazard ratios (HR) with 95% confidence intervals (CI); T and N, TNM7 primary tumor and lymph node stage. (**D** and **E**) Immunodetection of SPP1 protein (brown) in lungs from naïve C57BL/6 mice ($n = 5$; D) and from urethane-treated (10 weekly intraperitoneal injections of 1 g/kg; latency 6 months) C57BL/6 mice competent ($Spp1^{+/+}$; $n = 23$) or deficient ($Spp1^{-/-}$; $n = 19$) in both Spp1 alleles (E) shows high expression by nonciliated airway epithelial cells (red arrows), alveolar epithelial cells (magenta arrows), alveolar macrophages (blue arrows), and lung tumor cells (yellow arrows) selectively from $Spp1^{+/+}$ mice. Inlays, isotype controls. (**F**) Bronchoalveolar lavage (BAL) SPP1 protein levels from urethane-treated C57BL/6 mice competent ($Spp1^{+/+}$), haploinsufficient ($Spp1^{+/-}$), or deficient ($Spp1^{-/-}$) in Spp1 alleles at 0 ($n = 5$/group), 1 ($n = 7$–9/group), and 6 ($n = 5$–8/group) months post-treatment start shows increased SPP1 elaboration into the airspaces during chemical carcinogenesis. Dots, mean; bars, SD; *n*, sample size; *P*, 2-way ANOVA probability; ***, $P < 0.001$ for $Spp1^{+/+}$ mice at indicated time-points compared with time-point 0 months. (**G** and **H**) Microarray (**G**) and qPCR (**H**) results of relative abundance of SPP1 and its receptors' transcripts in RNA extracted from naïve FVB mouse lungs, urethane-exposed FVB mouse lungs at 1 week post 1 g/kg urethane, and primary LADC cells derived from urethane-induced lung tumors ((22); GSE94981; **G**, $n = 2$/group; **H**, $n = 3$/group) identify and validate overexpression of Spp1, Itgav, Itgb1, Itgb3, Itgb5, and Cd44 (grey area) by LADC cells relative to Gusb housekeeping transcript. Dots, mean; bars, SD; *n*, sample size; *P*, 2-way ANOVA probability. (**I**) Representative integrin-β3 (ITGB3) immunoreactivity (green) of naïve murine lungs and primary LADC cells derived from urethane-induced lung tumors ($n = 5$/group) counterstained with Hoechst 33258 (blue).

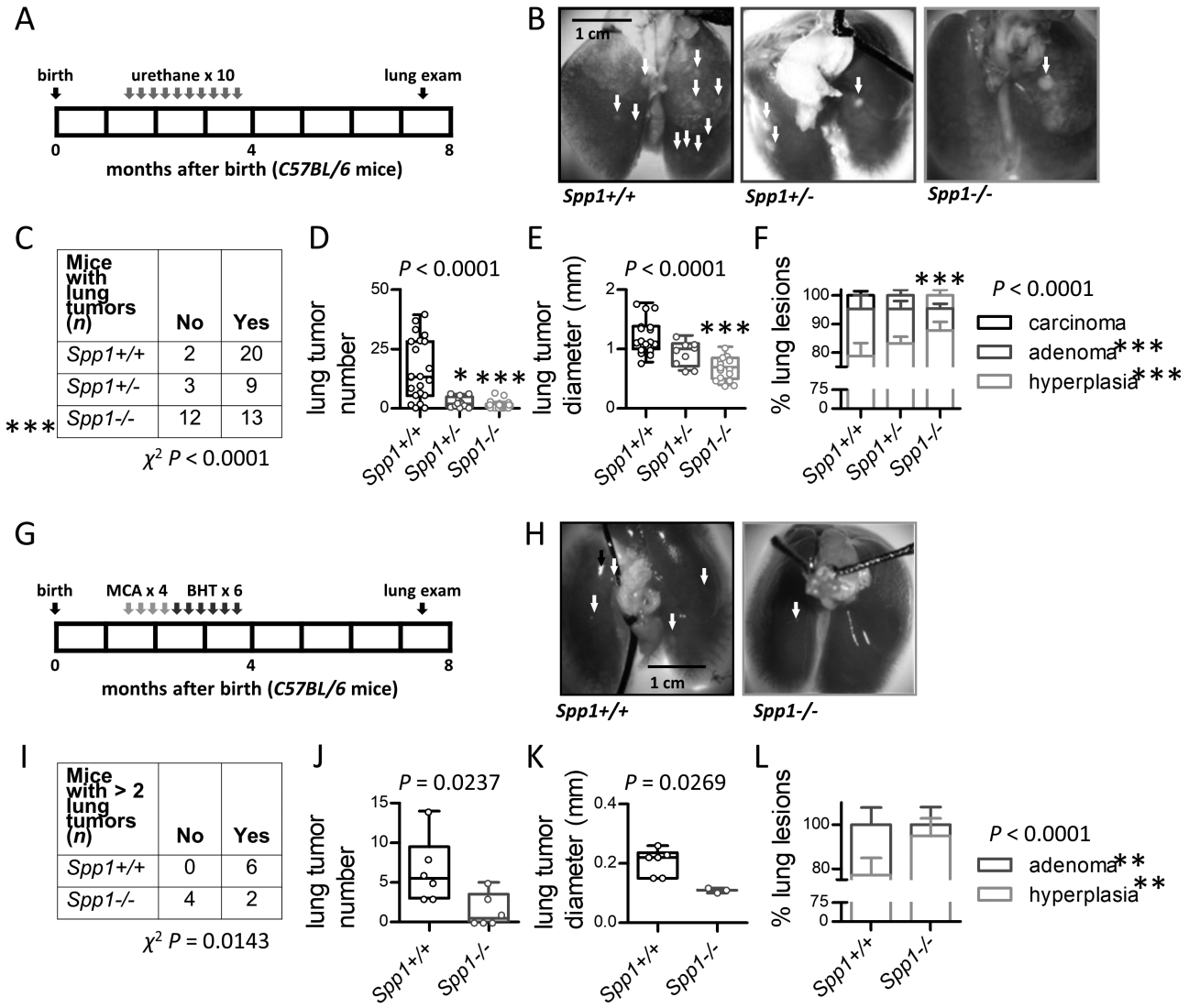

Figure 2. SPP1 promotes chemical-induced lung carcinogenesis. (**A–F**) *Spp1*$^{+/+}$, *Spp1*$^{+/-}$, and *Spp1*$^{-/-}$ mice on the *C57BL/6* background were treated with urethane and were sacrificed 6 months post-urethane start for assessment of pulmonary oncogenesis. Shown are experimental schematic with each box representing 1 month (**A**), photographs of representative lungs with tumors (**B**, arrows), as well as data summary of mouse numbers (*n*) and tumor incidence (**C**), number of lung tumors (**D**), diameter of lung tumors (**E**), and histologic distribution of neoplastic lesions (**F**). *n*, sample size; *circles*, data points; *lines*, median; *boxes*, interquartile range; *bars*, 50% outer quartiles; *P*, overall probability by χ^2 test (**C**), Kruskal–Wallis test (**D** and **E**), and 2-way ANOVA (**F**); * and ***, $P < 0.05$ and $P < 0.001$, respectively, for comparison of the indicated group with *Spp1*$^{+/+}$ mice by Fischer's exact test (**C**), Dunn's multiple comparison test (**D** and **E**), and Bonferroni post-test (**F**). (**G–L**) *Spp1*$^{+/+}$ and *Spp1*$^{-/-}$ mice on the *C57BL/6* background were treated with 3-methylcholanthrene (MCA) followed by butylated hydroxytoluene (BHT) and were sacrificed 6 months post-MCA start for assessment of pulmonary oncogenesis. Shown are experimental schematic with each box representing 1 month (**G**), photographs of representative lungs with tumors (**H**, arrows), as well as data summary of mouse numbers (*n*) and tumor incidence (**I**), number of lung tumors (**J**), diameter of lung tumors (**K**), and histologic distribution of neoplastic lesions (**L**) according to Ref. (36). *n*, sample size; *circles*, data points; *lines*, median; *boxes*, interquartile range; *bars*, 50% outer quartiles; *P*, overall probability by χ^2 test (**I**), Mann–Witney *U*-test (**J** and **K**), and 2-way ANOVA (**L**); **$P < 0.01$ for comparison of the indicated group with *Spp1*$^{+/+}$ mice by Bonferroni post-test (**L**).

use HEK293T embryonic kidney cells, a cell line that is easily transfected and does not bear mutant *Kras* or any syngeneic mutations in the *Egfr-Kras* pathway in order to have an insight into a more close to human approach. We first optimized transient transfection protocols of HEK293T cells with a p*GFP* eukaryotic expression vector, obtaining >90% transfection efficiency using >10 ng DNA/2 × 10^4 cells at 96 h (Figure 5A and B). HEK293T cells were subsequently stably transfected with p*GFP* or p*RFP*, followed by transient transfection with vectors encoding mutant murine *Kras*^{G12C} and/or murine SPP1, mixing of equal numbers of p*GFP* (test) and p*RFP* (control)-expressing cells, and co-culture for 1 week in *in vitro* competition assays. Alternatively, co-incubation for 1 week with rmSPP1 or anti-human α-SPP1 was performed. Quantification of pGFP+ and pRFP+ cells by fluorescent microscopy and flow cytometry revealed that forced overexpression of pΔ*Kras* alone impaired the survival of HEK293T cells, similar to our previous results with other cell lines (21). This pΔ*Kras*-induced anti-survival effect was completely preventable by p*Spp1* overexpression and by co-incubation with exogenous rmSPP1 and was further aggravated by co-incubation with α-SPP1 (Figure 5C–E). In a second experimental approach, *CAG-luc-eGFP* mice constitutively expressing *Photinus pyralis* luciferase in all somatic cells ((27); *FVB* strain) received a single intraperitoneal injection of urethane (1 g/kg), were sacrificed after 2 weeks (when *Kras* mutations occur in the lungs (38); and single cell suspensions of pulmonary

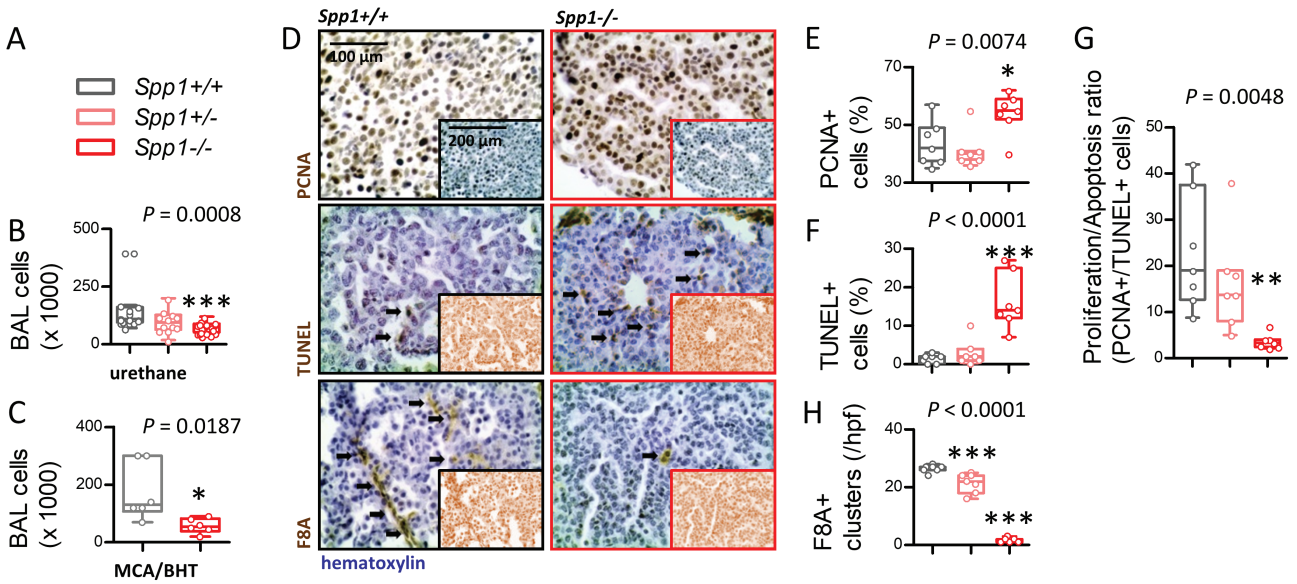

Figure 3. SPP1 fosters inflammation, neovascularization, and cancer cell survival in de novo lung tumors. *Spp1*$^{+/+}$, *Spp1*$^{+/-}$, and *Spp1*$^{-/-}$ mice on the *C57BL/6* background were treated with urethane or 3-methylcholanthrene (MCA) followed by butylated hydroxytoluene (BHT) and were sacrificed 6 months post-treatment start as in Figure 2A and G, respectively. (**A**) Legend to experimental groups. Nucleated cell numbers of bronchoalveolar lavage (n = 16, 12, and 25, respectively, for *Spp1*$^{+/+}$, *Spp1*$^{+/-}$, and *Spp1*$^{-/-}$ mice treated with urethane (**B**) and n = 6/group for *Spp1*$^{+/+}$ and *Spp1*$^{-/-}$ mice treated with MCA/BHT, (**C**). Shown are representative images (**D**) from the immunoreactivity (brown color; arrows) of lung tumors from urethane-treated mice for proliferating cell nuclear antigen (PCNA, top), terminal deoxynucleotidyl nick-end labeling (TUNEL, middle), and factor VIII-related antigen (F8A, bottom) protein expression (blue color indicates hematoxylin counterstain), and data summary (**E–G**) from n = 7 mice/group (10 different tumors from each mouse were examined and averaged). *Inlays*, isotype controls. *n*, sample size; *circles*, data points; *lines*, median; *boxes*, interquartile range; *bars*, 50% outer quartiles; *P*, overall probability, Unpaired *t*-test (**C**) and one-way ANOVA with Tuckey's Multiple Comparison Test (**B** and **E–G**); *, $P < 0.05$, **, $P < 0.01$, and ***, $P < 0.001$, respectively, for comparison of the indicated group with *Spp1*$^{+/+}$ mice by Dunn's multiple comparison test.

cells (50 000 cells/mouse) were incubated for 2 weeks with PBS control, rmSPP1, or anti-mouse α-SPP1. Bioluminescent detection of cell mass and cell counting revealed that exogenous rmSPP1 fostered and neutralization of endogenous SPP1 using α-SPP1 inhibited the survival of tumor-initiated pulmonary cells (Figure 5F–H). These results suggested that epithelial-derived SPP1 potentially selectively sustains the survival of *Kras*-mutant epithelial cells in an autocrine and/or paracrine fashion. To definitively test this, we stably transfected HEK293T cells with a vector encoding *P.pyralis* luciferase (p*Cag.Luc*) with or without p*ΔKras*, followed by transient transfections with a control (pC) or p*Spp1* vectors. Upon validation, 2 × 10^6 transfected cells were injected pairwise into the rear flanks of *NOD/SCID* mice followed by serial tumor measurements and bioluminescence imaging. As shown in Figure 6, p*ΔKras* or p*Spp1* alone did not render HEK293T cells tumorigenic, but simultaneous overexpression of p*ΔKras* and p*Spp1* resulted in formation of large primary tumors in 50% of the mice injected. These data corroborated that SPP1 can function as a promoter of *Kras*-mutant tumors *in vivo*.

SPP1 is required for KRAS^{G12D}-driven LADC

To further prove the pro-tumor effects of SPP1 on *KRAS*-mutant tumors, we generated intercrosses of mice conditionally expressing mutant *KRAS*^{G12D} upon CRE-mediated recombination (*LSL.KRAS*^{G12D}; (26)) with *Spp1*$^{+/+}$, *Spp1*$^{+/-}$, and *Spp1*$^{-/-}$ mice. The transgenic mice received intratracheally Ad-*Cre* and were sacrificed 4 months later. Similar to results from chemical models, *Spp1* gene-deficiency was protective from *KRAS*^{G12D}-driven LADC (Figure 6H and K). To strengthen our findings using additional models, but also to highlight the possible autocrine effects of SPP1, *LSL.KRAS*^{G12D} mice were intercrossed with mice conditionally overexpressing SPP1 upon CRE-mediated recombination (*LSL.SPP1*^{Tg}; (29)) and offsprings received 5 × 10^8 PFU Ad-*Cre* and were sacrificed 3 months later. In this model, oncogenic *KRAS*^{G12D} and SPP1 were co-expressed sporadically in the respiratory epithelium. Again, SPP1 overexpression specifically in *KRAS*^{G12D}-initiated cells (see Supplementary Figure 2, available at *Carcinogenesis* Online) markedly enhanced carcinogenesis (Figure 6J and L), solidifying the link between SPP1 and mutant *KRAS*.

Discussion

In the present study, we investigated the functional role of SPP1 in autochthonous airway epithelial carcinogenesis induced by two different tobacco chemicals and by oncogenic mutant *KRAS*^{G12D}. In accord with previous studies, analyses of multiple published datasets confirmed the marked (>25-fold) overexpression of SPP1 in LADC compared with adjacent non-tumorous lung tissues, as well as its importance in predicting poor survival (13,39–41). Our findings are the first to demonstrate that SPP1 is overexpressed and required for murine LADC induction by two different tobacco carcinogens. Collectively, the data presented support that lung epithelial SPP1 sustains the survival of *KRAS*-mutant lung epithelial cells at early time points post-carcinogen exposure, while myeloid-secreted SPP1 drives tumor-associated inflammation. Finally, an unequivocal role for SPP1 as a tumor promoter in the cellular context of mutant *KRAS* is shown using xenotransplant models and mouse models of stochastic *KRAS* mutation infliction in the murine respiratory epithelium.

Epithelial SPP1 is shown here to function in a cell-autonomous fashion to drive the survival of *KRAS*-mutated lung epithelial cells. This is supported by the decreased cellular proliferation and the increased apoptosis of epithelial cells in the

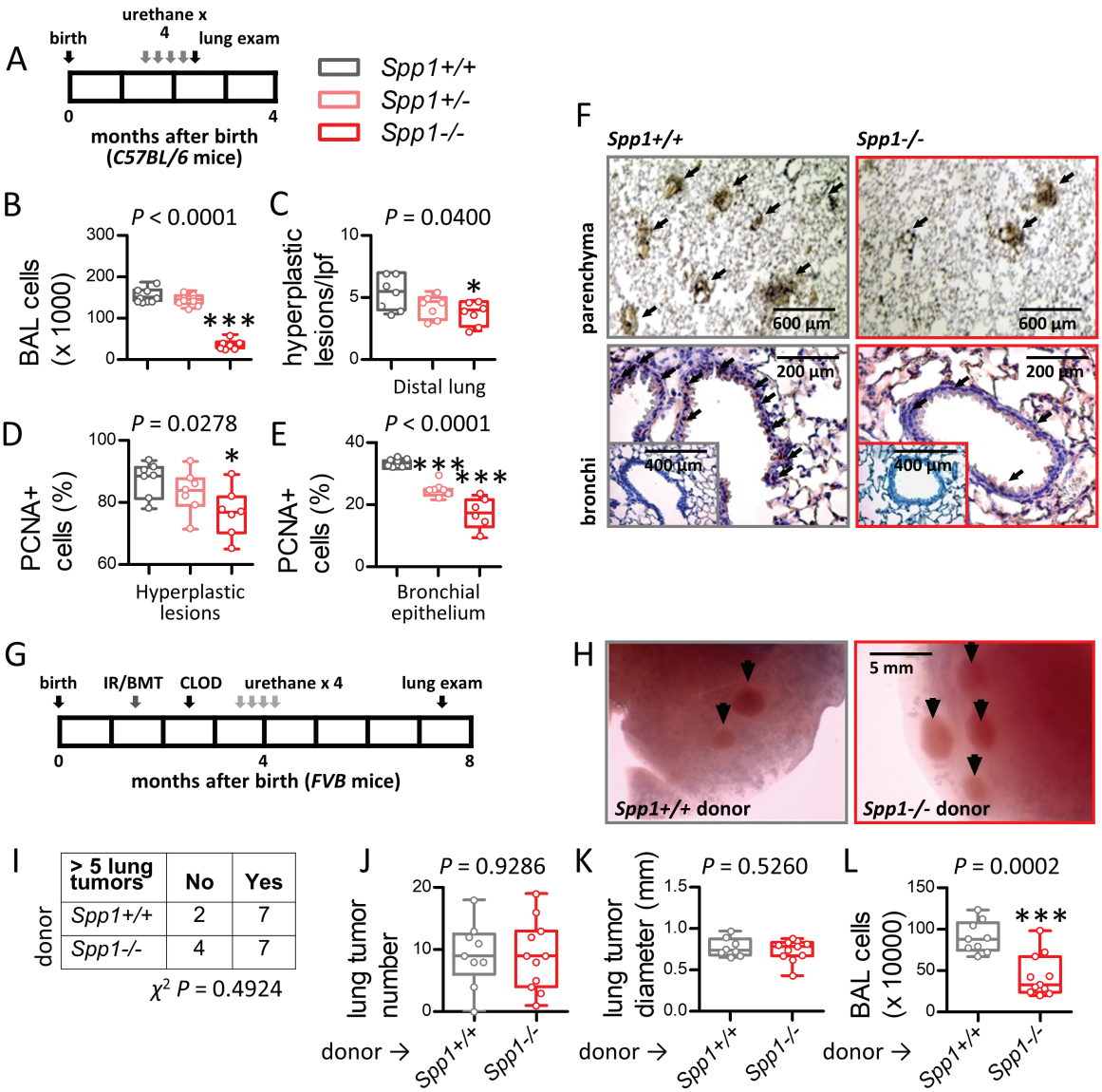

Figure 4. Epithelial-derived SPP1 drives preneoplasia in the tumor-initiated lung. (**A–F**) *Spp1*$^{+/+}$(*n* = 9), *Spp1*$^{+/-}$ (*n* = 9), and *Spp1*$^{-/-}$ (*n* = 7) mice on the *C57BL/6* background were treated with urethane and were sacrificed 1 month post-treatment start. Shown are experimental schematic with each box representing 1 month (**A**), data summary of nucleated cell numbers of bronchoalveolar lavage (**B**), number of atypical alveolar hyperplastic lesions (**C**), proliferating cell nuclear antigen (PCNA) immunoreactive cell abundance within these lesions (**D**), and PCNA immunoreactive cell abundance in airway epithelium (**E**), as well as representative images of PCNA immunoreactivity of alveolar (top) and airway (bottom) regions (**F**). *Inlays*, isotype controls; *n*, sample size; *circles*, data points; *lines*, median; *boxes*, interquartile range; *bars*, 50% outer quartiles; *P*, overall probability by Kruskal–Wallis test; * and ***, $P < 0.05$ and $P < 0.001$, respectively, for comparison of the indicated group with *Spp1*$^{+/+}$ mice by Dunn's multiple comparison test. (**G–L**) *FVB* mice received total body irradiation (900 rad, IR) followed by same-day bone marrow transplants (10 million cells flushed from the four long bones; BMT) from *Spp1*$^{+/+}$ and *Spp1*$^{-/-}$ mice. After 1 month necessary for bone marrow reconstitution, chimeras received intratracheal clodronate aimed at alveolar macrophage depletion and their reconstitution by bone marrow-derived chimeric macrophages, which is complete after another month (31), when animals received urethane and were sacrificed 6 months post-urethane start for assessment of pulmonary oncogenesis. Shown are experimental schematic with each box representing 1 month (**G**), photographs of representative lungs with tumors (**H**, arrows), as well as data summary of mouse numbers (*n*) and tumor incidence (**I**), number of lung tumors (**J**), diameter of lung tumors (**K**), and nucleated cell numbers of bronchoalveolar lavage (**L**). *n*, sample size; *circles*, data points; *lines*, median; *boxes*, interquartile range; *bars*, 50% outer quartiles; *P*, overall probability by χ^2 test (**I**) and Mann–Witney *U*-test (**J–L**).

lungs of *Spp1*-gene-deficient mice upon carcinogen exposure, by the survival advantage of cells co-expressing mutant KRAS and SPP1 *in vitro* and *in vivo*, and by the results from genetic models where $KRAS^{G12D}$ and SPP1 expression were stochastically inflicted in the same cells across the lung epithelium. This mechanism of SPP1 effects in LADC is plausible, since pulmonary tumor initiated cells expressed at the same time SPP1 and a battery of its receptors' transcripts, including *Itgav*, *Itgb1*, *Itgb3*, *Itgb5*, and *Cd44*. In particular integrinβ3 (ITGB3), which was validated at the protein level to be focally expressed by the respiratory epithelium and lung tumors in our chemical models, was recently shown to drive lung tumor cell stemness and drug resistance by interacting with oncogenic *KRAS* to promote non-canonical activation of nuclear factor (NF)-κB (42). Hence, SPP1 and ITGB3 signaling might be the missing link between *KRAS* mutations and alternative NF-κB pathway activation that we recently reported in patients and mice with LADC (17,22,23,43). Our results are also in line with the role of SPP1 in causing the radiation

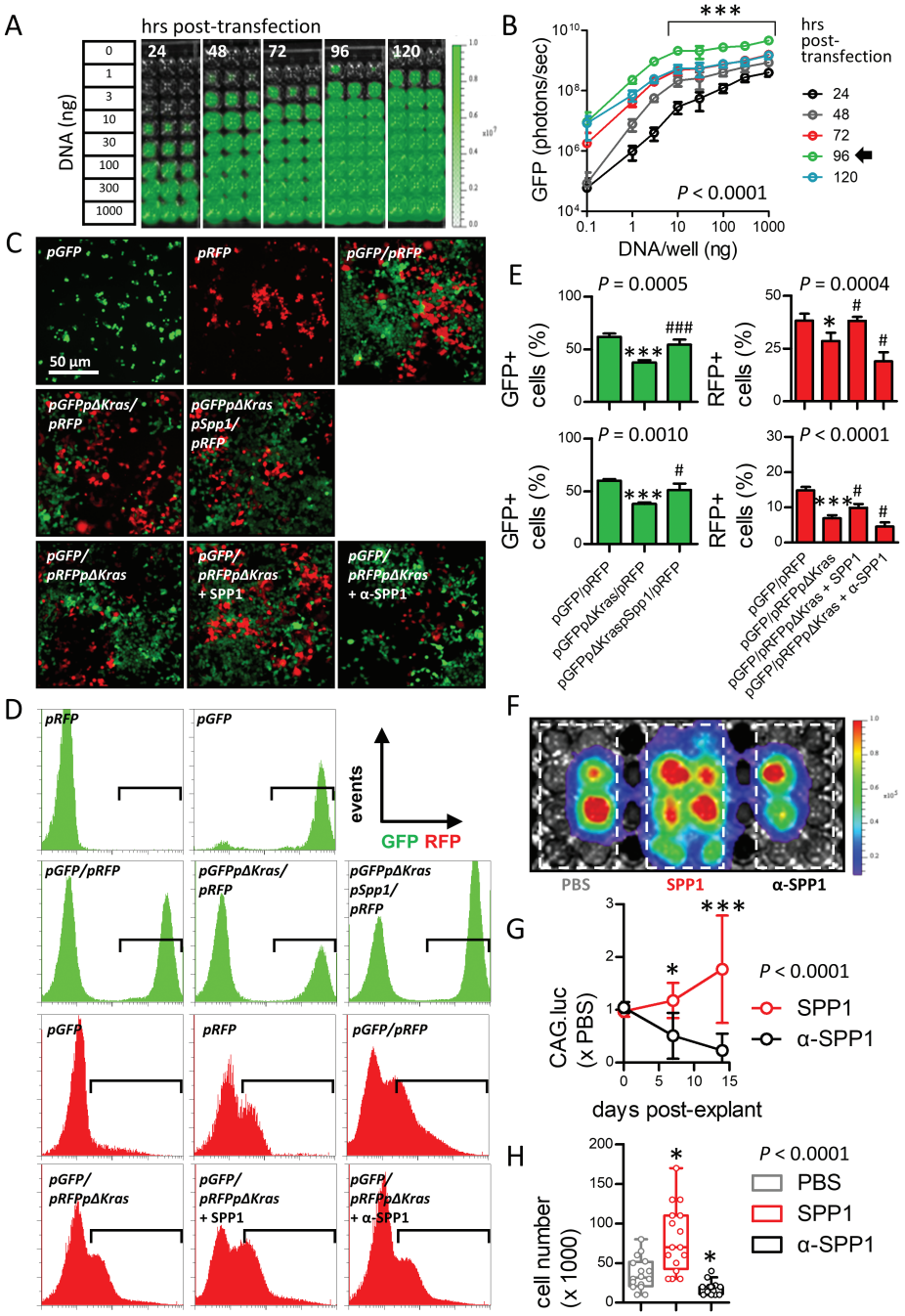

Figure 5. SPP1 fosters the survival of KRAS-mutant cells. (**A** and **B**) HEK293T benign human embryonic kidney cells were transiently transfected with varying amounts of a eukaryotic expression vector encoding enhanced GFP and green fluorescence was quantified by serial biofluorescence imaging of live cells. Shown are representative biofluorescence images (**A**) and summary of data from $n = 3$ independent experiments (**B**). *Circles*, mean; *bars*, SD; *n*, sample size; *P*, 2-way ANOVA probability; ***, $P < 0.001$ for plasmid amounts ≥ 10 ng/well at 96 h compared with all other time-points and with 0 ng/well DNA. (**C–E**) HEK293T cells were stably transfected with eukaryotic expression vectors encoding enhanced GFP (p*GFP*) or RFP (p*RFP*). Thereafter, p*GFP*-expressing cells were transiently transfected with eukaryotic expression vectors encoding mutant murine *Kras*(p*ΔKras*) alone or p*ΔKras* plus murine SPP1 (p*Spp1*), were mixed with equal numbers of p*RFP*-expressing HEK293T cells, co-cultured for 1 week, and finally were quantified by fluorescent microscopy and flow cytometry. Alternatively, p*RFP*-expressing cells were transiently transfected with p*ΔKras*, mixed with equal numbers of p*GFP*-expressing cells, and were co-incubated for 1 week with recombinant murine SPP1 (rmSPP1; 40 ng/ml) or neutralizing anti-SPP1 antibody (α-SPP1; 10 μg/ml) followed by cell quantification. Shown are representative fluorescent microscopic images (**C**) and flow cytometry histograms (**D**), as well as data summary from $n = 3$ independent experiments (**E**). *n*, sample size; *columns*, mean; *bars*, SD; *P*, overall probability by one-way ANOVA; * and ***, $P < 0.05$ and $P < 0.001$, respectively, for comparison of the indicated groups with p*GFP*/p*RFP* control co-cultures by Tukey's multiple comparison test; * and ***, $P < 0.05$ and $P < 0.001$, respectively, for comparison of the indicated groups with p*GFP*p*ΔKras*/p*RFP* or p*GFP*/p*RFP*p*ΔKras* co-cultures by Tukey's multiple comparison test. (**F**–**H**) *LSL.R26.Luc* mice (*FVB* background; $n = 8$) received a single intraperitoneal injection of urethane (1 g/kg), were sacrificed after 2 weeks (when *Kras* mutations occur in the lungs), and single cell suspensions of pulmonary cells were plated (20 000 cells from each mouse/96-well) and incubated for 2 weeks with PBS control, rmSPP1 (10 ng/ml), or α-SPP1 (10 μg/ml). Cell mass was quantified longitudinally using bioluminescence imaging and after 2 weeks using cell counting. Shown are representative bioluminescence image (**F**), as well as data summary from $n = 8$ independent experiments (**G** and **H**). (**G**) *Circles*, mean; *bars*, SD; *P*, 2-way ANOVA probability; * and ***, $P < 0.05$ and $P < 0.001$, respectively for rmSPP1-treated cells at indicated time-points compared with α-SPP1-treated cells. (**H**) *circles*, data points; *lines*, median; *boxes*, interquartile range; *bars*, 50% outer quartiles; *P*, overall probability by Kruskal–Wallis test; *, $P < 0.05$ for comparison of the indicated groups with PBS-treated cells by Dunn's post-test.

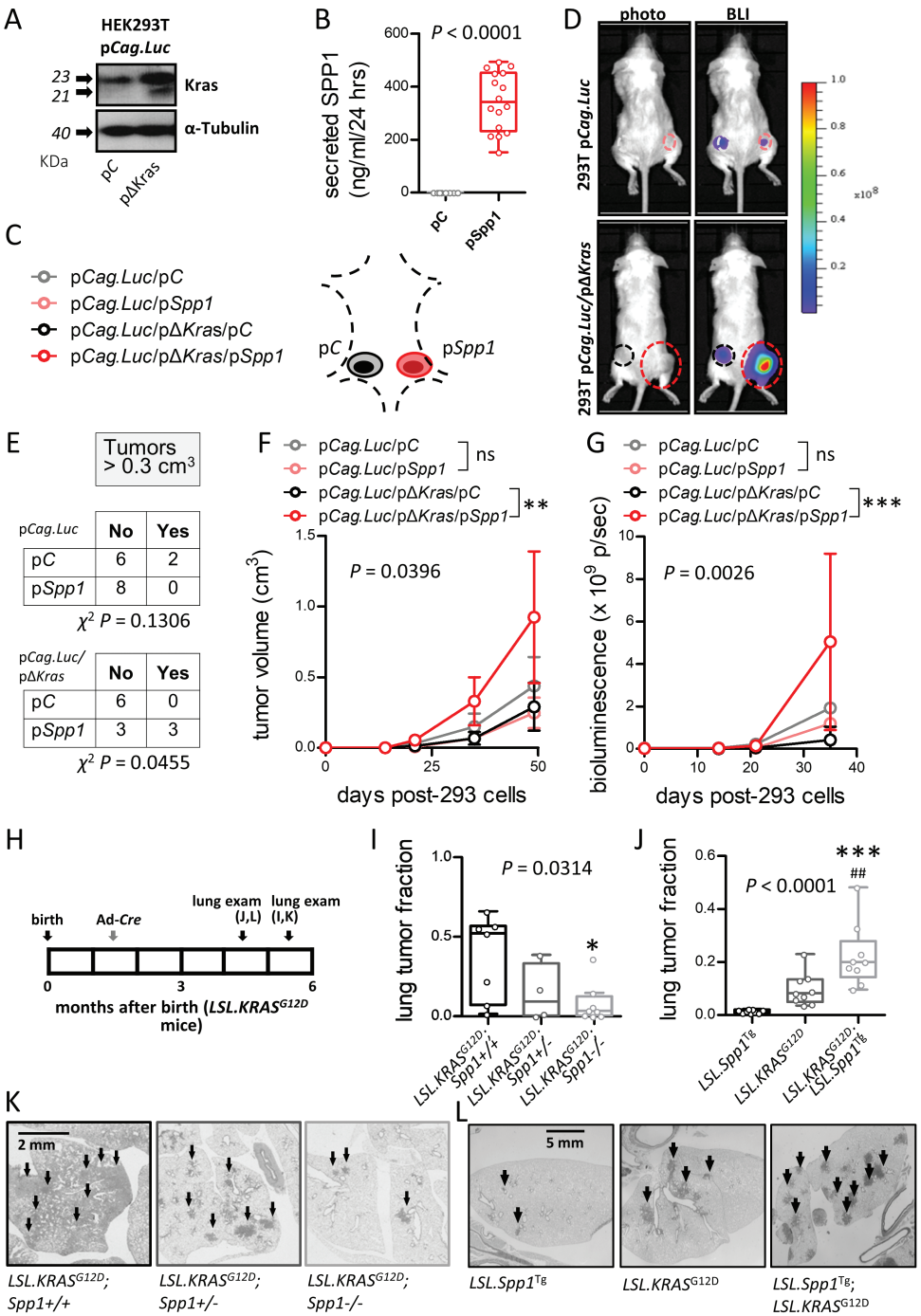

Figure 6. SPP1 drives de novo tumorigenesis in the cellular context of mutant KRAS. HEK293T cells were stably transfected with a eukaryotic expression vector encoding *Photinus pyralis* luciferase (p*Cag.Luc*) alone or in combination with mutant murine Kras (p*ΔKras*). Thereafter, pools of 3–5 stable clones were transiently transfected with random sequence control (pC) or murine SPP1 (p*Spp1*) plasmids, were validated, and 2 × 10^6 cells expressing pC or p*Spp1* were injected pairwise into the rear flanks of *NOD/SCID* mice followed by serial tumor measurements and bioluminescence imaging. (**A**) Cropped immunoblots of whole cell extracts probed with anti-Kras and anti-α-Tubulin antibodies. (**B**) SPP1 protein secretion by ELISA. *Circles*, data points; *lines*, median; *boxes*, interquartile range; *bars*, 50% outer quartiles; *P*, Mann–Whitney *U*-test probability. (**C**) Legend and schematic representation of experimental set-up. (**D**) Representative bioluminescence images of living mice at 35 days post-HEK293T cell injection. (**E**) Numbers of mice used and incidence of tumors larger than 0.3 cm^3. (**F**) Data summary of tumor volume. (**G**) Data summary of bioluminescence imaging. (**F** and **G**) *Circles*, mean; *bars*, SD; *P*, 2-way ANOVA probability; ns, **, and ***, $P > 0.05$, $P < 0.01$, and $P < 0.001$, respectively for the indicated comparisons at the final time-points. Mice conditionally expressing mutant $KRAS^{G12D}$ upon CRE-mediated recombination (*LSL.*$KRAS^{G12D}$) and simultaneously competent ($Spp1^{+/+}$; $n = 7$), haploinsufficient ($Spp1^{+/-}$;$n = 4$), or deficient ($Spp1^{-/-}$; $n = 8$) in *Spp1* alleles (all on the *C57BL/6* background) received 5 × 10^8 plaque-forming units (PFU) intratracheal adenovirus encoding CRE recombinase (Ad-*Cre*) and were sacrificed 4 months later (**I** and **K**). Alternatively, *LSL.*$KRAS^{G12D}$ mice were intercrossed with mice conditionally expressing SPP1 upon CRE-mediated recombination (*LSL.*$SPP1^{Tg}$) and offsprings *LSL.*$SPP1^{Tg}$ ($n = 9$), *LSL.*$KRAS^{G12D}$ ($n = 9$) and *LSL.*$KRAS^{G12D}$; *LSL.*$SPP1^{Tg}$ ($n = 9$) received 5 × 10^8 PFU Ad-*Cre* and were sacrificed 3 months later (**J** and **L**). Shown are experimental schematic with each box representing 1 month (**H**), data summary of mouse lung tumor fraction (**I** and **J**), as well as hematoxylin and eosin-stained representative lung tissue sections with tumors (**K**, **L**, arrows). *n*, sample size; *circles*, data points; *lines*, median; *boxes*, interquartile range; *bars*, 50% outer quartiles; *P*, overall probability by Kruskal–Wallis test; *, $P < 0.05$ for comparison of the indicated group with *LSL.*$KRAS^{G12D}$; $Spp1^{+/+}$ mice by Dunn's post-test (**B**); ***, $P < 0.001$ for comparison of the indicated group with *LSL.*$SPP1^{Tg}$ mice by Dunn's post-test; **, $P < 0.01$ for comparison of the indicated group with *LSL.*$KRAS^{G12D}$ mice by Dunn's post-test.

resistance of *KRAS*-mutated lung cancers (44) and with the effects of CD44, another SPP1 receptor, in driving *KRAS*-mutant lung cancers (15,45). Taken together, our results explain previous links of SPP1 to enhanced lung cancer progression and pin the cytokine's pro-tumor functions to a defined molecular subclass of this cancer type, that is, *KRAS*-mutant LADCs of smokers.

One of the most interesting findings from adoptive bone marrow transplant experiments was that selectively SPP1 of epithelial origin fuels chemical-induced LADC development, while myeloid-derived SPP1 participates in mounting tumor-associated inflammation without impacting carcinogenesis. The latter observation does not provide experimental support to a report of increased macrophage SPP1 expression in lung cancer patients, which was correlated with poor survival (40). Notwithstanding a potential tumor-promoting effect of immune-derived SPP1 in lung cancer not evident in the bone marrow transplant model employed here, our studies highlight the prime mechanism of the pro-tumorigenic functions of SPP1 in the lungs: SPP1 expressed by the tumor-initiated pulmonary epithelium promotes the survival of transformed cells that harbor *KRAS* mutations. To this end, recent and earlier studies in patients with lung cancer have underlined SPP1 as a peripheral blood biomarker of disease progression and response to therapy (39–41,46,47) and their findings can be explained by the tissue-restricted effects of epithelial SPP1 reported here. The latter can be explained by different isoforms of SPP1 potentially secreted by epithelial and myeloid cells, as well as the differential effects of the cytokine depending on cellular *TP53* mutation status (11). The known facts that mature chemical-induced LADC commonly carry deleted or mutated *Trp53* alleles (18,48), and that SPP1 functions to promote cellular survival especially in the cellular context of functional, wild-type *TP53* alleles (11), further supports our findings of early effects of SPP1 post-carcinogen exposure.

Our findings have explicit clinical implications and we hope that they will prompt clinical progress aimed at inhibiting SPP1 in lung cancer, in addition to using it as a biomarker of tumor mass, survival, and therapy response (39,40,46). Despite potential therapeutic applications in patients with established malignant lung tumors, we believe that the major potential clinical application of our findings would be SPP1-targeted chemoprevention strategies to prevent LADC development in smokers. This is feasible given the multitude of the agents available to inhibit SPP1 signaling (16,29,46). The concept of lung cancer chemoprevention targeted at tumor-associated inflammation is an emerging certainty in the field after the results of the Canakinumab Anti-inflammatory Thrombosis Outcomes Study (CANTOS) trial: neutralization of interleukin-1β using the humanized monoclonal antibody canakinumab aimed at reduction of cardiovascular risk achieved its primary endpoint by decreasing cardiovascular events by up to 15% (49), at the same time inadvertently decreasing lung cancer mortality in the high-dose intervention group by an astonishing 77% (50). We believe that SPP1 could be an equally lucrative target for chemoprevention of incident LADC in ever smokers at high risk for the disease. In conclusion, osteopontin is shown to play a pivotal tumor promoting role in early stages of LADC development. Evidence from multiple mouse models and from humans is presented that pins the cytokine as a prime target for chemoprevention of LADC in the lungs of smokers.

Supplementary material

Supplementary data are available at *Carcinogenesis* online.

Funding

This work was supported by a Grant from the Hellenic Thoracic Society and by the European Research Council 2010 Starting Independent Investigator and 2015 Proof of Concept Grants (260524 and 679345, respectively, to GTS). I.G. is a recipient of a Greek State Scholarship Foundation (IKY) programme co-financed by the European Union (European Social Fund-ESF), by Greek national funds through an action entitled "Reinforcement of Postdoctoral Researchers" (NSRF 2014 – 2020). I. Psallidas is the recipient of a REPSIRE2 European Respiratory Society Fellowship (grant number 2015–7160).

Authors' contribution

IG performed *in vivo* experiments, histology, and wrote the first draft of the manuscript; NIK did microarrays and qPCR; IL did immunohistochemistry and morphometry; VP performed *in vitro* GFP-reporter assays; DMS generated/contributed SPP1-deleted mice; ADG, CM, AM, SM, IK performed *in vivo* experiments, VP contributed conditional SPP1-overexpressing mice; ASL analyzed human survival/ microarray data; DEZ performed immunofluorescence; TA generated eukaryotic expression vectors; GTS analyzed all data and created the figures; GTS and PI designed, wrote the final version of the manuscript, and are the guarantors of the study's integrity. All authors critically reviewed the paper for important intellectual content and approved the final submitted version.

Conflict of Interest Statement: None declared.

References

1. Fitzmaurice, C. *et al.* (2017) Global, regional, and national cancer incidence, mortality, years of life lost, years lived with disability, and disability-adjusted life-years for 32 cancer groups, 1990 to 2015: a systematic analysis for the global burden of disease study. *JAMA Oncol.*, 3, 524–548.
2. Collisson, E.A. (2014) Comprehensive molecular profiling of lung adenocarcinoma. *Nature*, 511, 543–550.
3. Bender, E. (2014) Epidemiology: the dominant malignancy. *Nature*, 513, S2–S3.
4. Alberg, A.J. *et al.* (2007) Epidemiology of lung cancer: ACCP evidence-based clinical practice guidelines (2nd edition). *Chest*, 132(3 Suppl), 29S–55S.
5. Stephen, A.G. *et al.* (2014) Dragging ras back in the ring. *Cancer Cell*, 25, 272–281.
6. Nadal, E. *et al.* (2014) KRAS-G12C mutation is associated with poor outcome in surgically resected lung adenocarcinoma. *J. Thorac. Oncol.*, 9, 1513–1522.
7. Ashkar, S. *et al.* (2000) Eta-1 (osteopontin): an early component of type-1 (cell-mediated) immunity. *Science*, 287, 860–864.
8. Yin, M. *et al.* (2014) Osteopontin promotes the invasive growth of melanoma cells by activating integrin αvβ3 and down-regulating tetraspanin CD9. *Am. J. Pathol.*, 184, 842–858.
9. Sangaletti, S. *et al.* (2014) Osteopontin shapes immunosuppression in the metastatic niche. *Cancer Res.*, 74, 4706–4719.
10. Psallidas, I. *et al.* (2013) Secreted phosphoprotein-1 directly provokes vascular leakage to foster malignant pleural effusion. *Oncogene*, 32, 528–535.
11. Giopanou, I. *et al.* (2017) Tumor-derived osteopontin isoforms cooperate with TRP53 and CCL2 to promote lung metastasis. *Oncoimmunology*, 6, e1256528.
12. Khodavirdi, A.C. *et al.* (2006) Increased expression of osteopontin contributes to the progression of prostate cancer. *Cancer Res.*, 66, 883–888.
13. Shi, S.M. *et al.* (2016) Increased osteopontin protein expression may be correlated with poor prognosis in non-small-cell lung cancer: a meta analysis. *J. Cancer Res. Ther.*, 12, 277–282.

14. Sun, B.S. *et al.* (2013) Osteopontin knockdown suppresses non-small cell lung cancer cell invasion and metastasis. *Chin. Med. J. (Engl).*, 126, 1683–1688.
15. Zhao, P. *et al.* (2013) CD44 promotes Kras-dependent lung adenocarcinoma. *Oncogene*, 32, 5186–5190.
16. Minai-Tehrani, A. *et al.* (2013) Aerosol delivery of lentivirus-mediated O-glycosylation mutant osteopontin suppresses lung tumorigenesis in K-ras (LA1) mice. *Cell. Oncol. (Dordr).*, 36, 15–26.
17. Stathopoulos, G.T. *et al.* (2007) Epithelial NF-kappaB activation promotes urethane-induced lung carcinogenesis. *Proc. Natl Acad. Sci. USA*, 104, 18514–18519.
18. Westcott, P.M. *et al.* (2015) The mutational landscapes of genetic and chemical models of Kras-driven lung cancer. *Nature*, 517, 489–492.
19. Kabbout, M. *et al.* (2013) ETS2 mediated tumor suppressive function and MET oncogene inhibition in human non-small cell lung cancer. *Clin. Cancer Res.*, 19, 3383–3395.
20. Győrffy, B. *et al.* (2013) Online survival analysis software to assess the prognostic value of biomarkers using transcriptomic data in non-small-cell lung cancer. *PLoS One*, 8, e82241.
21. Agalioti, T. *et al.* (2017) Mutant KRAS promotes malignant pleural effusion formation. *Nat. Commun.*, 8, 15205.
22. Vreka, M. *et al.* (2018) IκB Kinase α Is required for development and progression of KRAS-mutant lung adenocarcinoma. *Cancer Res.*, 78, 2939–2951.
23. Marazioti, A. *et al.* (2018) Myeloid-derived interleukin-1β drives oncogenic KRAS-NF-κB addiction in malignant pleural effusion. *Nat. Commun.*, 9, 672.
24. Giannou, A.D. *et al.* (2017) NRAS destines tumor cells to the lungs. *EMBO Mol. Med.*, 9, 672–686.
25. Liaw, L. *et al.* (1998) Altered wound healing in mice lacking a functional osteopontin gene (spp1). *J. Clin. Invest.*, 101, 1468–1478.
26. Jackson, E.L. *et al.* (2001) Analysis of lung tumor initiation and progression using conditional expression of oncogenic K-ras. *Genes Dev.*, 15, 3243–3248.
27. Safran, M. *et al.* (2003) Mouse reporter strain for noninvasive bioluminescent imaging of cells that have undergone Cre-mediated recombination. *Mol. Imaging*, 2, 297–302.
28. Blunt, T. *et al.* (1995) Defective DNA-dependent protein kinase activity is linked to V(D)J recombination and DNA repair defects associated with the murine scid mutation. *Cell*, 80, 813–823.
29. Kourepini, E. *et al.* (2014) Osteopontin expression by CD103- dendritic cells drives intestinal inflammation. *Proc. Natl Acad. Sci. USA*, 111, E856–E865.
30. Zaynagetdinov, R. *et al.* (2012) Epithelial nuclear factor-κB signaling promotes lung carcinogenesis via recruitment of regulatory T lymphocytes. *Oncogene*, 31, 3164–3176.
31. Everhart, M.B. *et al.* (2005) Intratracheal administration of liposomal clodronate accelerates alveolar macrophage reconstitution following fetal liver transplantation. *J. Leukoc. Biol.*, 77, 173–180.
32. Faul, F. *et al.* (2007) G*Power 3: a flexible statistical power analysis program for the social, behavioral, and biomedical sciences. *Behav. Res. Methods*, 39, 175–191.
33. Uhlen, M. *et al.* (2017) A pathology atlas of the human cancer transcriptome. *Science*, 357, eaan2507.
34. Rud, A.K. *et al.* (2013) Osteopontin is a prognostic biomarker in non-small cell lung cancer. *BMC Cancer*, 13, 540.
35. Hu, Z. *et al.* (2005) Overexpression of osteopontin is associated with more aggressive phenotypes in human non-small cell lung cancer. *Clin. Cancer Res.*, 11, 4646–4652.
36. Nikitin, A.Y. *et al.* (2004) Classification of proliferative pulmonary lesions of the mouse: recommendations of the mouse models of human cancers consortium. *Cancer Res.*, 64, 2307–2316.
37. Karabela, S.P. *et al.* (2011) Neutralization of tumor necrosis factor bioactivity ameliorates urethane-induced pulmonary oncogenesis in mice. *Neoplasia*, 13, 1143–1151.
38. Ichikawa, T. *et al.* (1996) The activation of K-ras gene at an early stage of lung tumorigenesis in mice. *Cancer Lett.*, 107, 165–170.
39. Blasberg, J.D. *et al.* (2010) Reduction of elevated plasma osteopontin levels with resection of non-small-cell lung cancer. *J. Clin. Oncol.*, 28, 936–941.
40. Yan, C.H. *et al.* (2015) Osteopontin is a novel prognostic biomarker in early-stage non-small cell lung cancer after surgical resection. *J. Cancer Res. Clin. Oncol.*, 141, 1371–1378.
41. Ouyang, X. *et al.* (2018) Osteopontin promotes cancer cell drug resistance, invasion, and lactate production and is associated with poor outcome of patients with advanced non-small-cell lung cancer. *Onco. Targets. Ther.*, 11, 5933–5941.
42. Seguin, L. *et al.* (2014) An integrin β_3-KRAS-RalB complex drives tumour stemness and resistance to EGFR inhibition. *Nat. Cell Biol.*, 16, 457–468.
43. Giopanou, I. *et al.* (2015) Comprehensive evaluation of nuclear factor-κB expression patterns in non-small cell lung cancer. *PLoS One*, 10, e0132527.
44. Wang, M. *et al.* (2017) Radiation resistance in KRAS-mutated lung cancer is enabled by stem-like properties mediated by an osteopontin-EGFR pathway. *Cancer Res.*, 77, 2018–2028.
45. Talekar, M. *et al.* (2016) Combination wt-p53 and MicroRNA-125b transfection in a genetically engineered lung cancer model using dual CD44/EGFR-targeting Nanoparticles. *Mol. Ther.*, 24, 759–769.
46. Mack, P.C. *et al.* (2008) Lower osteopontin plasma levels are associated with superior outcomes in advanced non-small-cell lung cancer patients receiving platinum-based chemotherapy: SWOG Study S0003. *J. Clin. Oncol.*, 26, 4771–4776.
47. Li, Y. *et al.* (2015) Osteopontin-expressing macrophages in non-small cell lung cancer predict survival. *Ann. Thorac. Surg.*, 99, 1140–1148.
48. Gao, W. *et al.* (2017) KRAS and TP53 mutations in bronchoscopy samples from former lung cancer patients. *Mol. Carcinog.*, 56, 381–388.
49. Ridker, P.M. *et al.* (2017) Effect of interleukin-1β inhibition with canakinumab on incident lung cancer in patients with atherosclerosis: exploratory results from a randomised, double-blind, placebo-controlled trial. *Lancet*, 390, 1833–1842.
50. Ridker, P.M. *et al.* (2017) Antiinflammatory therapy with canakinumab for atherosclerotic disease. *N. Engl. J. Med.*, 377, 1119–1131.